CHALMERS
FINITE ELEMENT CENTER

PREPRINT 2002–14

On adaptive strategies and error control in fracture mechanics

Per Heintz and Klas Samuelsson

Chalmers Finite Element Center
CHALMERS UNIVERSITY OF TECHNOLOGY
Göteborg Sweden 2002

CHALMERS FINITE ELEMENT CENTER

Preprint 2002–14

On adaptive strategies and error control in fracture mechanics

Per Heintz and Klas Samuelsson

CHALMERS

Chalmers Finite Element Center
Chalmers University of Technology
SE–412 96 Göteborg Sweden
Göteborg, October 2002

On adaptive strategies and error control in fracture mechanics
Per Heintz and Klas Samuelsson
NO 2002–14
ISSN 1404–4382

Chalmers Finite Element Center
Chalmers University of Technology
SE–412 96 Göteborg
Sweden
Telephone: +46 (0)31 772 1000
Fax: +46 (0)31 772 3595
`www.phi.chalmers.se`

Printed in Sweden
Chalmers University of Technology
Göteborg, Sweden 2002

ON ADAPTIVE STRATEGIES AND ERROR CONTROL IN FRACTURE MECHANICS

PER HEINTZ AND KLAS SAMUELSSON

ABSTRACT. Finite element approximations in elastic fracture mechanics are traditionally carried out on a priori constructed meshes with singularity elements that surrounds the crack tip. In this contribution we discuss an adaptive algorithm based on goal oriented error measures using ordinary elements and a p-refinement for the linearization of the secant forms. The numerical experiments show that good results can be obtained without imposition of hands before the computations starts. Furthermore, we note that it is often possible, for engineering goal quantities, to linearize the data to the dual problem such that additional discretization error is avoided, and the error representation formula is in a sense trivial.

1. INTRODUCTION

Specifying a goal quantity a priori makes it possible to formulate a corresponding dual problem that describes the error transport in the domain, related to the particular quantity of interest. The dual problem can be approximated numerically and further used in an adaptive algorithm in order to adapt the mesh to the pre-specified goal, i.e., *goal oriented adaptivity.* A posteriori error estimates based on duality was introduced in the 1990:s by Johnson and co-workers [3, 2, 1] and have also been used in nonlinear solid mechanics by Rannacher and co-workers in [4, 5]. See also Larsson et al. [6] for further developments.

In this contribution we propose an adaptive algorithm based on a global p-refinement of the primal problem. The finer approximation is used in the linearization of the secant form of the error measure. We show that the error representation formula for the error in the goal quantity turns out to be trivial if the dual problem is then approximated in the same p-refined function space. We also consider using the results from the finer primal problem.

Prediction of instability of a preexisting macroscopic crack is often based on the assumption that the material in the vicinity of the crack behaves in a linear elastic fashion, so that the stress field has a singularity at the crack tip. The crack is defined as being unstable when the stress intensity reaches a critical material dependent level, and is traditionally obtained from the FE approximation by studying crack boundary movements or using an integral formulation of the energy release rate at crack growth. Although much research

---

Date: October 21, 2002.

Key words and phrases. Adaptivity, Fracture mechanics, Energy release rate.

Per Heintz, Department of Applied Mechanics, Chalmers University of Technology, S–412 96 Göteborg, Sweden, *email*: per.heintz@me.chalmers.se

Klas Samuelsson, Department of Mathematics, Chalmers University of Technology, S–412 96 Göteborg, Sweden, *email*: klassam@math.chalmers.se.

has been done in this field there is little attention paid to the analysis of discretization errors in the FE approximation. For instance, the design of the finite element mesh is often made a priori instead of using adaptive techniques. In the numerical experiments we investigate how well the adaptive algorithm resolves approximations encountered in fracture mechanics. We do not use special singularity elements or other special techniques since the purpose is to exploit the nature of the algorithm in a fundamental fashion. For background material on the considered energy release rate methods we refer to [7], [8] and [9].

The outline of the paper is as follows: In section 2 we recall the Gateaux derivative and the nonlinear Galerkin orthogonality which are essential to the error analysis on which the adaptive algorithm is based. In section 3 we derive the error representation formula, based on duality arguments, for an arbitrary choice of goal functional. Furthermore we discuss how the continuous dual problem can be linearized in a computational setting. In section 4 we describe the adaptive strategy and mention some different mesh refinement options. In section 5, a model problem is formulated and we present the considered goal quantities used in the simulations. In section 6 we present our numerical results and finally, in section 7, we present some concluding remarks.

2. Preliminaries

In the following sections we denote a test function $\boldsymbol{v}$ and a direction of the Gateaux derivative $\boldsymbol{w}$. The d-dimensional function space $\boldsymbol{V}$ is defined as

$$\boldsymbol{V} \overset{\text{def}}{=} \{v_i : \int v_i^2 + |\nabla v_i|^2 < \infty, i = 1, \dots, d\},$$

with corresponding finite element subspace $\boldsymbol{V}_h$.

The variational and FE formulation of a linear PDE is described in terms of its bilinear $a(\boldsymbol{u},\boldsymbol{v})$ and linear form $L(\boldsymbol{v})$; find $\boldsymbol{u} \in \boldsymbol{V},\ \boldsymbol{u}_h \in \boldsymbol{V}_h$:

$$a(\boldsymbol{u},\boldsymbol{v}) = L(\boldsymbol{v}) \qquad \forall \boldsymbol{v} \in \boldsymbol{V}, \tag{2.1}$$

$$a(\boldsymbol{u}_h,\boldsymbol{v}) = L(\boldsymbol{v}) \qquad \forall \boldsymbol{v} \in \boldsymbol{V}_h. \tag{2.2}$$

The Galerkin orthogonality for linear operators is obtained subtracting (2.2) from (2.1)

$$a(\boldsymbol{e},\boldsymbol{v}) = 0 \qquad \forall \boldsymbol{v} \in \boldsymbol{V}_h, \tag{2.3}$$

where $\boldsymbol{e} \overset{\text{def}}{=} \boldsymbol{u} - \boldsymbol{u}_h$. For nonlinear operators, the corresponding variational and FE formulation reads; find $\boldsymbol{u} \in \boldsymbol{V},\ \boldsymbol{u}_h \in \boldsymbol{V}_h$:

$$a(\boldsymbol{u};\boldsymbol{v}) = L(\boldsymbol{v}) \qquad \forall \boldsymbol{v} \in \boldsymbol{V}, \tag{2.4}$$

$$a(\boldsymbol{u}_h;\boldsymbol{v}) = L(\boldsymbol{v}) \qquad \forall \boldsymbol{v} \in \boldsymbol{V}_h, \tag{2.5}$$

where $a(\cdot;\cdot)$ is the semi linear form (nonlinear in the test and linear in the trial argument).

The Gateaux derivative of the semi linear form with respect to its first argument is defined as

$$a'(\boldsymbol{u};\boldsymbol{w},\boldsymbol{v}) \overset{\text{def}}{=} \frac{\partial}{\partial \epsilon} a(\boldsymbol{u}+\epsilon\boldsymbol{w};\boldsymbol{v})_{|\epsilon=0}. \tag{2.6}$$

The secant form of $a(\boldsymbol{u};\boldsymbol{v})$ is now obtained as

$$a_s(\boldsymbol{u},\boldsymbol{u}_h;\boldsymbol{w},\boldsymbol{v}) \overset{\text{def}}{=} \int_0^1 a'(\bar{\boldsymbol{u}}(s);\boldsymbol{w},\boldsymbol{v})\,ds, \tag{2.7}$$

where $\bar{\boldsymbol{u}}(s) \overset{\text{def}}{=} \boldsymbol{u}_h + s\boldsymbol{e}$. The choice $\boldsymbol{w}=\boldsymbol{e}$ leads to

$$a_s(\boldsymbol{u},\boldsymbol{u}_h;\boldsymbol{e},\boldsymbol{v}) = \int_0^1 a'(\bar{\boldsymbol{u}}(s);\boldsymbol{e},\boldsymbol{v})\,ds = a(\boldsymbol{u};\boldsymbol{v}) - a(\boldsymbol{u}_h;\boldsymbol{v}). \tag{2.8}$$

The nonlinear Galerkin orthogonality is now formulated using (2.4) to substitute the first term in (2.8)

$$a_s(\boldsymbol{u},\boldsymbol{u}_h;\boldsymbol{e},\boldsymbol{v}) = L(\boldsymbol{v}) - a(\boldsymbol{u}_h;\boldsymbol{v}) \qquad \forall \boldsymbol{v}\in\boldsymbol{V}, \tag{2.9}$$

$$a_s(\boldsymbol{u},\boldsymbol{u}_h;\boldsymbol{e},\boldsymbol{v}) = 0 \qquad \forall \boldsymbol{v}\in\boldsymbol{V}_h. \tag{2.10}$$

3. Error analysis based on duality

3.1. **The error representation formula.** Let $Q(\boldsymbol{u})$ be a quantity of physical interest derived from the solution $\boldsymbol{u}$. To measure the error in the discretization we introduce $E(\boldsymbol{u},\boldsymbol{u}_h)$ as

$$E(\boldsymbol{u},\boldsymbol{u}_h) \overset{\text{def}}{=} Q(\boldsymbol{u}) - Q(\boldsymbol{u}_h). \tag{3.1}$$

To establish the variational format of the dual problem, on which the a posteriori error estimate is based, we use the Gateaux derivative for $E(\boldsymbol{u},\boldsymbol{u}_h)$ with respect to its first argument

$$E'(\boldsymbol{u},\boldsymbol{u}_h;\boldsymbol{w}) \overset{\text{def}}{=} \frac{\partial}{\partial\epsilon}E(\boldsymbol{u}+\epsilon\boldsymbol{w},\boldsymbol{u}_h)\mid_{\epsilon=0} = \nabla Q(\boldsymbol{u})\cdot\boldsymbol{w}. \tag{3.2}$$

We now define the secant form of $E(\boldsymbol{u},\boldsymbol{u}_h)$ as

$$E_S(\boldsymbol{u},\boldsymbol{u}_h;\boldsymbol{w}) \overset{\text{def}}{=} \int_0^1 E'(\bar{\boldsymbol{u}}(s),\boldsymbol{u}_h;\boldsymbol{w})ds = \int_0^1 \nabla Q(\bar{\boldsymbol{u}}(s))\cdot\boldsymbol{w}\,ds, \tag{3.3}$$

The choice $\boldsymbol{w}=\boldsymbol{e}$ leads to

$$E_S(\boldsymbol{u},\boldsymbol{u}_h;\boldsymbol{e}) = E(\boldsymbol{u},\boldsymbol{u}_h) - E(\boldsymbol{u}_h,\boldsymbol{u}_h) = E(\boldsymbol{u},\boldsymbol{u}_h). \tag{3.4}$$

For given $\boldsymbol{u}$ and $\boldsymbol{u}_h$ we recall the secant form of the primal problem (2.7), and define the corresponding dual bilinear form $a_S^*(\boldsymbol{u},\boldsymbol{u}_h;\boldsymbol{w},\boldsymbol{v})$ such that

$$a_S^*(\boldsymbol{u},\boldsymbol{u}_h;\boldsymbol{w},\boldsymbol{v}) \overset{\text{def}}{=} a_S(\boldsymbol{u},\boldsymbol{u}_h;\boldsymbol{v},\boldsymbol{w}). \tag{3.5}$$

The variational format of the dual problem is now formulated as; find $\boldsymbol{\varphi}\in\boldsymbol{V}$:

$$a_S^*(\boldsymbol{u},\boldsymbol{u}_h;\boldsymbol{\varphi},\boldsymbol{v}) = E_S(\boldsymbol{u},\boldsymbol{u}_h,\boldsymbol{v}) \qquad \forall\boldsymbol{v}\in\boldsymbol{V}. \tag{3.6}$$

Using (3.5), (3.6) and (2.9) the following exact error representation holds where we have chosen $\boldsymbol{v}=\boldsymbol{e}$

$$\begin{aligned} E_S(\boldsymbol{u},\boldsymbol{u}_h;\boldsymbol{e}) &= a_S^*(\boldsymbol{u},\boldsymbol{u}_h;\boldsymbol{\varphi},\boldsymbol{e}) = a_S(\boldsymbol{u},\boldsymbol{u}_h;\boldsymbol{e},\boldsymbol{\varphi}) \\ &= a_S(\boldsymbol{u};\boldsymbol{e},\boldsymbol{u}_h,\boldsymbol{\varphi}-\pi_h\boldsymbol{\varphi}) = L(\boldsymbol{\varphi}-\pi_h\boldsymbol{\varphi}) - a(\boldsymbol{u}_h;\boldsymbol{\varphi}-\pi_h\boldsymbol{\varphi}). \end{aligned} \tag{3.7}$$

The third equality is obtained using the Galerkin orthogonality (2.10) to insert an interpolant $\pi_h \boldsymbol{\varphi}$ that belongs to $\boldsymbol{V}_h$.

Using (3.4) and (3.1) we obtain

$$\begin{aligned} E(\boldsymbol{u}, \boldsymbol{u}_h) &= L(\boldsymbol{\varphi} - \pi_h \boldsymbol{\varphi}) - a(\boldsymbol{u}_h, \boldsymbol{\varphi} - \pi_h \boldsymbol{\varphi}) \\ &= \sum_{K \in T_h} (L(\boldsymbol{\varphi} - \pi_h \boldsymbol{\varphi}) - a(\boldsymbol{u}_h, \boldsymbol{\varphi} - \pi_h \boldsymbol{\varphi}))_K, \end{aligned} \tag{3.8}$$

$$|E(\boldsymbol{u}, \boldsymbol{u}_h)| = |\sum_{K \in T_h} (L(\boldsymbol{\varphi} - \pi_h \boldsymbol{\varphi}) - a(\boldsymbol{u}_h, \boldsymbol{\varphi} - \pi_h \boldsymbol{\varphi}))_K|, \tag{3.9}$$

where the summation is carried out over every element K in the mesh T_h. Equation (3.9) is the exact error representation formula that will be used in the adaptive routine.

Remark: For two chosen function spaces, $\boldsymbol{V}_h$ and a larger discrete function space $\boldsymbol{V}_{h^+}$, $E_S(\boldsymbol{u}, \boldsymbol{u}_h; \boldsymbol{v})$ can be linearized exactly for goal quantities that are at most quadratic in $\boldsymbol{u}$ (since the gradient is then linear in $\boldsymbol{u}$). The error representation formula for bilinear forms, with $\boldsymbol{\varphi} \in \boldsymbol{V}_{h^+}$, is thus trivial with respect to the considered function spaces.

3.2. **Discretizing the dual problem.** Solving the dual problem (3.6) first requires a linearization of the functional $E_S(\boldsymbol{u}, \boldsymbol{u}_h; \boldsymbol{v})$. Nonlinear error measures can be linearized using the *rectangle* (3.10), *trapezoidal* (3.11) or *midpoint* (3.12) rule.

$$\int_0^1 \nabla Q(\bar{\boldsymbol{u}}(s)) \cdot \boldsymbol{w} \, ds \approx \nabla Q(\boldsymbol{u}_h) \cdot \boldsymbol{w}, \tag{3.10}$$

$$\int_0^1 \nabla Q(\bar{\boldsymbol{u}}(s)) \cdot \boldsymbol{w} \, ds \approx \frac{\nabla Q(\boldsymbol{u}_h) + \nabla Q(\boldsymbol{u}_{h^+})}{2} \cdot \boldsymbol{w}, \tag{3.11}$$

$$\int_0^1 \nabla Q(\bar{\boldsymbol{u}}(s)) \cdot \boldsymbol{w} \, ds \approx \nabla Q\left(\frac{\boldsymbol{u}_h}{2} + \frac{\boldsymbol{u}_{h^+}}{2}\right) \cdot \boldsymbol{w}, \tag{3.12}$$

where $\boldsymbol{u}_{h^+}$ is an improved solution closer to $\boldsymbol{u}$, computed in a larger function space $\boldsymbol{V}_{h^+}$.

The Galerkin orthogonality (2.10) forces the discrete solution to the dual problem to belong to a different function space than $\boldsymbol{V}_h$. Using the same enlarged function space as above we thus consider the following function spaces:

$$\boldsymbol{V}_h \subset \boldsymbol{V}_{h^+} \subset \boldsymbol{V}. \tag{3.13}$$

Carrying out the discretization we obtain the discretized dual problem; find $\boldsymbol{\varphi} \in \boldsymbol{V}_{h^+}$:

$$a_S^*(\boldsymbol{u}_{h^+}, \boldsymbol{u}_h; \boldsymbol{\varphi}, \boldsymbol{v}) = E_S(\boldsymbol{u}_{h^+}, \boldsymbol{u}_h; \boldsymbol{v}) \qquad \forall \boldsymbol{v} \in \boldsymbol{V}_{h^+}. \tag{3.14}$$

Since $\boldsymbol{V}_{h^+} \subset \boldsymbol{V}$, the exact error representation (3.9) must now be replaced by an approximate one:

$$|E(\boldsymbol{u}, \boldsymbol{u}_h)| \approx |\sum_{K \in T_h} (L(\boldsymbol{\varphi}_{h^+} - \pi_h \boldsymbol{\varphi}) - a(\boldsymbol{u}_h, \boldsymbol{\varphi}_{h^+} - \pi_h \boldsymbol{\varphi}))_K|. \tag{3.15}$$

A straightforward way to choose $\boldsymbol{V}_{h^+}$ is to use one order higher finite elements than was used when discretizing the primal problem, or a refined triangulation with the same order. To reduce the overhead cost, simplified methods based on solving the dual problem in $\boldsymbol{V}_h$

followed by post-processing to obtain a $\boldsymbol{\varphi}$ that belongs to an improved space have been proposed; see for instance [6] for developments in this direction. In this paper we will use p-refinement. This might seem costly, but on the other hand the computations also yields the result of the finer primal problem. This is clearly a more accurate solution which can be used instead of the coarse one. The only drawback is that we do not have as correct error representation for the fine solution as for the coarse solution.

4. Refinement strategy

Starting from (3.9) the following estimates of the error holds

$$
\begin{aligned}
|E(\boldsymbol{u},\boldsymbol{u}_h)| &= |\sum_{K\in T_h} (L(\boldsymbol{\varphi}-\pi_h\boldsymbol{\varphi}) - a(\boldsymbol{u}_h,\boldsymbol{\varphi}-\pi_h\boldsymbol{\varphi}))_K|, && (4.1)\\
&\leq \sum_{K\in T_h} |(L(\boldsymbol{\varphi}-\pi_h\boldsymbol{\varphi}) - a(\boldsymbol{u}_h,\boldsymbol{\varphi}-\boldsymbol{\pi_h}\boldsymbol{\varphi}))|_K, && (4.2)\\
&\leq \sum_{K\in T_h} R_K(\boldsymbol{u}_h)\cdot W_K(\boldsymbol{\varphi}-\pi_h\boldsymbol{\varphi}). && (4.3)
\end{aligned}
$$

Equation (4.1) is an identity and in (4.2), the triangle inequality supresses cancellation between different elements. In (4.3) integration by parts together with the Cauchy-Schwarz inequality results in two constants R_K and W_K on the element level, e.g., with $a(\boldsymbol{u},\boldsymbol{v}) = \int (A\boldsymbol{u})\cdot\boldsymbol{v}$ and $L(\boldsymbol{v}) = \int \boldsymbol{f}\cdot\boldsymbol{v}$,

$$
\begin{aligned}
R_K(\boldsymbol{u}_h) &= ||\boldsymbol{R}_h||_{L_2(K)} && (4.4)\\
W_K(\boldsymbol{\varphi}-\pi_h\boldsymbol{\varphi}) &= ||\boldsymbol{\varphi}-\pi_h\boldsymbol{\varphi}||_{L_2(K)}, && (4.5)
\end{aligned}
$$

where $\boldsymbol{R}_h \overset{\text{def}}{=} A\boldsymbol{u}_h - \boldsymbol{f}$. In earlier work [10] there has been proposed the use of (4.1) as a stop criterion and (4.2) for assigning refinement indicators to the elements in T_h. This is a natural choice since elements with large contributions to (4.1) must be controlled. The weights used in (4.3) can be used to compute indicators and error bounds, but the obtained bound could be many times larger than $|E(\boldsymbol{u},\boldsymbol{u}_h)|$ [10].

Furthermore, the set of element errors from (4.2) can be used in different ways when choosing specific elements to refine. We mention three strategies together with some comments. We define η_K as the error contribution from element K and the corresponding indicator as $I_K = |\eta_K|$.

1. *Fixed fraction.* In each refinement cycle the elements are sorted according to their indicator's magnitude I_K and a fixed fraction are chosen to be refined. This strategy gives good control of the size of the refined mesh, but is insensitive to whether the problem has a singularity or not. Over refinements when singularities are present is common in practice.
2. *Relative fraction.* In each refinement cycle the elements are sorted according to their indicator's magnitude I_K and each element, whose indicator value is greater than or equal to a fraction of the largest value, is chosen to be refined. This strategy is more adaptive than strategy (1) and in practice, when a singularity is present,

the elements surrounding the singularity are chosen to be refined. If the threshold fraction is set to low, this strategy leads to many grid levels with just a few more elements from one level to the next.

(3) *Mixed refinement* Using this strategy a refinement flag between 0 and 3 is assigned to each element in the mesh. The flag indicates how many element sides that is to be divided to the next grid level. The breakpoint for flag $n \in \{1, 2, 3\}$ is defined by the parameter $r \in [0, 1]$ and the largest indicator value $I^{\max}_{K \in T_h}$ in the mesh, using the following formula

$$I^{\max}_{K \in T_h} \cdot r^{3-n} \geq I_K \geq r^{4-n} \cdot I^{\max}_{K \in T_h}. \tag{4.6}$$

5. Numerical experiments - a single edge notch

The primal problem is solved numerically on a grid hierarchy using h-refinement between each grid level. On each grid level we use a uniform p-refinement to obtain an improved solution $\boldsymbol{u}_{h^+} \in \boldsymbol{V}_{h^+}$ closer to $\boldsymbol{u}$. This improved solution is used in the linearization of $E_S(\boldsymbol{u}, \boldsymbol{u}_h; \boldsymbol{v})$, and the dual problem is then approximated in the same function space $\boldsymbol{V}_{h^+}$. The error representation formula is evaluated and the elements that is to be refined are chosen according to the mixed refinement strategy.

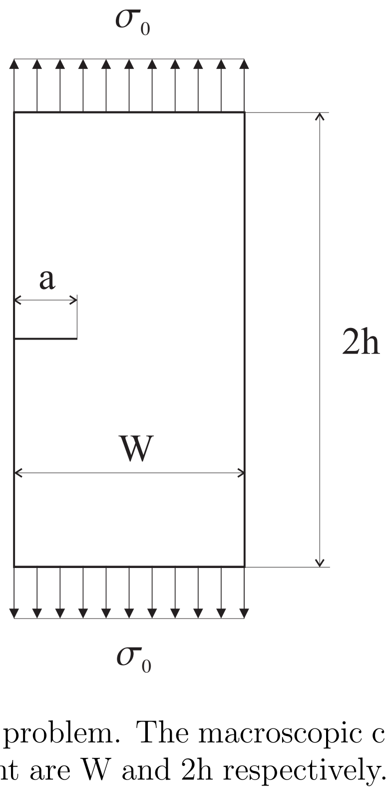

Figure 1. The primal problem. The macroscopic crack length is a, and the domain width and height are W and 2h respectively. The boundary traction is denoted by $\boldsymbol{\sigma_0}$.

5.1. **The primal problem.** Referring to Fig. 1 we solve, with $a = 0.1$m, $W = 0.5$m and $h = \{0.5, 1\}$m, the equations of linear elasticity with a prescribed boundary traction $\boldsymbol{\sigma}_0 = [0, 1\text{e}{+}06]$ N. The body is in plane stress, the crack is sharp and the Lamé coefficients are $\lambda = 121.154\text{e}{+}9$ and $\mu = 80.7692\text{e}{+}9$ corresponding to $E = 210\text{e}{+}06$ Pa and $\nu = 0.3$.

$$\boldsymbol{\sigma} = \lambda(\boldsymbol{\nabla} \cdot \boldsymbol{u})\boldsymbol{I} + 2\mu\boldsymbol{\varepsilon}(\boldsymbol{u}) \quad \text{in } \Omega, \tag{5.1}$$

$$-\boldsymbol{\nabla} \cdot \boldsymbol{\sigma}^T = \boldsymbol{f} \quad \text{in } \Omega, \tag{5.2}$$

$$\boldsymbol{u} = \boldsymbol{g} \quad \text{on } \partial\Omega_D, \tag{5.3}$$

$$\boldsymbol{\sigma} \cdot \boldsymbol{n} = \boldsymbol{\sigma_0} \quad \text{on } \partial\Omega_N. \tag{5.4}$$

Equation (5.1) defines the constitutive relation between Cauchy's stress tensor and the strain field and (5.2) represents force equilibrium in the domain. Boundary conditions are imposed by (5.3) and (5.4) as prescribed displacements and tractions respectively. The weak formulation of (5.1)-(5.4) is; find $\boldsymbol{u} \in \boldsymbol{V}$:

$$\int_\Omega \boldsymbol{\sigma}(\boldsymbol{u}) : \boldsymbol{\varepsilon}(\boldsymbol{v})\, d\Omega = \int_\Omega \boldsymbol{f} \cdot \boldsymbol{v}\, d\Omega + \int_{\partial\Omega_N} \boldsymbol{\sigma}_0 \cdot \boldsymbol{v}\; ds \;\; \forall \boldsymbol{v} \in \boldsymbol{V}. \tag{5.5}$$

In the FE approximation we choose $\boldsymbol{V}_h$ as the space of continuous piecewise linear, -quadratic and -cubic basis functions.

5.2. **The dual problems.** The stress field near a crack tip can be divided into three basic types, each associated with a deformation mode, see Fig. 2. Mode I is associated with tensile opening where the crack faces move directly apart. Mode II is characterized by displacements in which the crack faces slide over one another perpendicular to the leading edge of the crack. In Mode III, the crack surfaces slide parallel to the leading edge. The superposition of these three modes is often sufficient to describe a general deformation in the vicinity of the crack.

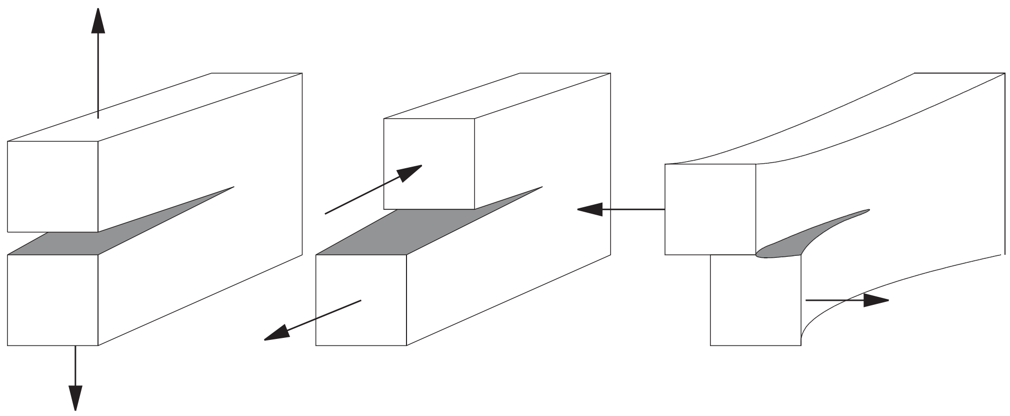

FIGURE 2. Deformation modes. 1) Mode I - tensile opening, 2) Mode II - in plane shear, and 3) Mode III - Out of plane shear.

The parameters K_I,K_{II} and K_{III} are the corresponding stress intensity factors associated with each deformation mode. Physically they represent the intensity of the linear-elastic stress distribution and from a mathematical point of view, the strengths of the $\frac{1}{\sqrt{r}}$ singularities at the crack tip. The stress intensity factors can be evaluated numerically from the displacement field or empirically from handbooks in fracture mechanics.

The relation between the stress intensity factors and the energy release rate at crack growth for a linear elastic specimen in plane stress is [11]

$$J = \frac{K_I^2}{E} + \frac{K_{II}^2}{E} + \frac{(1+\nu)K_{III}^2}{E}. \tag{5.6}$$

The corresponding energy release rate for our model problem is thus

$$J = \frac{K_I^2}{E}, \tag{5.7}$$

where the empirical expression for K_I is

$$K_I = \sqrt{\pi a} \cdot f(a, W), \tag{5.8}$$

with an accuracy better than 0.5% for any $\frac{a}{W}$ [11]. The term $f(a, W)$ is a geometry factor and it is noted that the stress intensity factor is a function of the loading conditions and geometry of the considered specimen only. The effect of $\frac{h}{W}$ is practically negligible for $\frac{h}{b} \geq 1.0$ [11]. The considered dimensions give the following expression for J

$$J = 2.7942 \pm 0.013971 \Longleftrightarrow J \in [2.7802, 2.808]. \tag{5.9}$$

In comparison with evaluating the stress intensity factors from the displacement field, the use of energy methods has the advantage that exact modeling of the crack tip behavior is not necessary.

In the following sections we consider three different goal quantities; crack boundary movements and two different integral formulations of the energy release rate J at crack growth. The dual problems are discretized with continuous piecewise polynomials of order $p+1$, where p is the order of the primal problem. The dual problems are on the form; find $\boldsymbol{\varphi} \in \boldsymbol{V}$:

$$a(\boldsymbol{\varphi}, \boldsymbol{v}) = E_S(\boldsymbol{u}, \boldsymbol{u}_h; \boldsymbol{v}) \qquad \forall \boldsymbol{v} \in \boldsymbol{V}. \tag{5.10}$$

Remark: Since the considered equations are linear and symmetric, the secant of the semi-linear form is simply $a_S^*(\boldsymbol{u}, \boldsymbol{u}_h; \boldsymbol{\varphi}, \boldsymbol{v}) = a(\boldsymbol{\varphi}, \boldsymbol{v})$.

5.2.1. *Crack boundary displacements.* We choose the mean vertical displacement along the upper crack boundary Γ_a as the goal quantity

$$Q(\boldsymbol{u}) = \frac{1}{|a|} \int_{\Gamma_a} \boldsymbol{u} \cdot n_2 \, ds, \tag{5.11}$$

where n_2 is the x_2 component of the unit normal on Γ_a and a is the crack length. The secant form is

$$E_S(\boldsymbol{u}, \boldsymbol{u}_h; \boldsymbol{v}) = \frac{1}{a} \int_{\Gamma_a} \boldsymbol{v} \cdot n_2 \, ds. \tag{5.12}$$

5.2.2. *Contour integral format.* The contour integral format of the energy release rate has been widely used as a fracture characterizing parameter. In 1968, Rice [7] showed that the value of this integral could be written as a path independent line integral for elastic materials, and thus could be evaluated at a remote contour avoiding singularity zones

$$Q(\boldsymbol{u}) = \int_\Gamma \left(W^e \, dx_2 - T_i \frac{\partial u_i}{\partial x_1} \, ds \right). \tag{5.13}$$

W^e is the elastic energy and $\boldsymbol{T} \overset{\text{def}}{=} \boldsymbol{\sigma} \cdot \boldsymbol{n}$ is the traction on the contour with normal $\boldsymbol{n}$. The corresponding secant form of the error measure is

$$E_S(\boldsymbol{u}, \boldsymbol{u}_h; \boldsymbol{v}) = \int_\Omega \int_0^1 \nabla Q(\bar{\boldsymbol{u}}) \cdot \boldsymbol{v} \, dS \, d\Omega, \tag{5.14}$$

where

$$\begin{aligned} &[\nabla Q(\bar{\boldsymbol{u}})]_1 = \\ &\quad \left(\frac{\partial \bar{u}_2}{\partial x_2} n_1 \lambda - n_2 \left(\frac{\partial \bar{u}_1}{\partial x_2} \mu + \frac{\partial \bar{u}_2}{\partial x_1} (\lambda + \mu) \right) \right) \frac{\partial (\cdot)}{\partial x_1} + \\ &\quad \left(\left(2 \frac{\partial \bar{u}_1}{\partial x_2} n_1 + \frac{\partial \bar{u}_2}{\partial x_1} n_1 - \frac{\partial \bar{u}_1}{\partial x_1} n_2 \right) \right) \mu \frac{\partial (\cdot)}{\partial x_2} \end{aligned} \tag{5.15}$$

$$\begin{aligned} &[\nabla Q(\bar{\boldsymbol{u}})]_2 = \\ &\quad \left(\frac{\partial \bar{u}_1}{\partial x_2} n_1 \mu - \frac{\partial \bar{u}_1}{\partial x_1} n_2 (\lambda + \mu) - \frac{\partial \bar{u}_2}{\partial x_2} n_2 (\lambda + 2\mu) \right) \frac{\partial (\cdot)}{\partial x_1} + \\ &\quad \left(\frac{\partial \bar{u}_1}{\partial x_1} n_1 \lambda + \left(2 \frac{\partial \bar{u}_2}{\partial x_2} n_1 - \frac{\partial \bar{u}_2}{\partial x_1} n_2 \right) (\lambda + 2\mu) \right) \frac{\partial (\cdot)}{\partial x_2} \end{aligned} \tag{5.16}$$

Remark: The secant form of the error measurer is linear both in $\bar{\boldsymbol{u}}$ and the test argument. It is thus possible to linearize $E_S(\boldsymbol{u}, \boldsymbol{u}_h; \boldsymbol{v})$ exactly between the function spaces $\boldsymbol{V}_h$ and $\boldsymbol{V}_{h^+}$ using the two primal solutions $\boldsymbol{u}_h$ and $\boldsymbol{u}_{h^+}$.

5.2.3. *Domain Integral format.* More recent formulations of the energy release rate apply an area integration (volume in 3D) for the energy release rate. Using Gauss' theorem and a scalar weight function q it is possible to rewrite the contour integral to an area integral [8]

$$Q(\boldsymbol{u}) = \int_A \left(\left[\sigma_{ij} \frac{\partial u_j}{\partial x_1} - W^e \delta_{1i} \right] \frac{\partial q}{\partial x_i} \right) dA. \tag{5.17}$$

The scalar function q equals one at the crack tip and zero at the contour Γ and A is the integration domain i.e. the area within the contour. The secant form of E is

$$E_S(\boldsymbol{u}, \boldsymbol{u}_h; \boldsymbol{v}) = \int_\Omega \int_0^1 \nabla Q(\bar{\boldsymbol{u}}) \cdot \boldsymbol{v} \, dS \, d\Omega, \tag{5.18}$$

where

$$
\begin{aligned}
&(\nabla Q(\bar{\boldsymbol{u}}))_1 = \\
&\quad \left(\frac{\partial q}{\partial x_2}\left(\mu\frac{\partial \bar{u}_1}{\partial x_2} + (\mu+\lambda)\frac{\partial \bar{u}_2}{\partial x_1}\right) - \lambda\frac{\partial \bar{u}_2}{\partial x_2}\frac{\partial q}{\partial x_1}\right)\frac{\partial(\cdot)}{\partial x_1} + \\
&\quad + \left(\mu\frac{\partial \bar{u}_1}{\partial x_1}\frac{\partial q}{\partial x_2} - \mu\frac{\partial q}{\partial x_1}\left(\frac{\partial \bar{u}_2}{\partial x_1} + 2\frac{\partial \bar{u}_1}{\partial x_2}\right)\right)\frac{\partial(\cdot)}{\partial x_2}
\end{aligned} \tag{5.19}
$$

$$
\begin{aligned}
&(\nabla Q(\bar{\boldsymbol{u}}))_2 = \\
&\quad \left(\frac{\partial q}{\partial x_2}\left(\frac{\partial \bar{u}_1}{\partial x_1}(\lambda+\mu) + \frac{\partial \bar{u}_2}{\partial x_2}(\lambda+2\mu)\right) - \frac{\partial q}{\partial x_1}\frac{\partial \bar{u}_1}{\partial x_2}\mu\right)\frac{\partial(\cdot)}{\partial x_1} + \\
&\quad + \left(\frac{\partial q}{\partial x_2}\frac{\partial \bar{u}_2}{\partial x_1}(\lambda+2\mu) - \frac{\partial q}{\partial x_1}\left(\frac{\partial \bar{u}_1}{\partial x_1}\lambda + 2\frac{\partial \bar{u}_2}{\partial x_2}(\lambda+2\mu)\right)\right)\frac{\partial(\cdot)}{\partial x_2}
\end{aligned} \tag{5.20}
$$

Remark: The secant form of the error measurer is linear both in $\bar{\boldsymbol{u}}$ and the test argument. It is thus possible to linearize $E_S(\boldsymbol{u}, \boldsymbol{u}_h; \boldsymbol{v})$ exact between the function spaces $\boldsymbol{V}_h$ and $\boldsymbol{V}_{h^+}$ using the two primal solutions $\boldsymbol{u}$ and $\boldsymbol{u}_{h^+}$.

6. NUMERICAL RESULTS

In this section we present computational results and convergence plots for each goal quantity and approximation order. In Fig. 3 we show the initial grids and in Fig. 4 the corresponding adapted grids for the considered goal quantities.

We use two effectivity indexes η_1 and η_2 defined as

$$\eta_1 = \frac{|\sum_{K\in T_h}(L(\boldsymbol{\varphi}_{h^+} - \pi_h\boldsymbol{\varphi}) - a(\boldsymbol{u}_h, \boldsymbol{\varphi}_{h^+} - \pi_h\boldsymbol{\varphi}))_K|}{Q(\boldsymbol{u}_{h^+}) - Q(\boldsymbol{u}_h)}, \tag{6.1}$$

$$\eta_2 = \frac{|\sum_{K\in T_h}(L(\boldsymbol{\varphi}_{h^+} - \pi_h\boldsymbol{\varphi}) - a(\boldsymbol{u}_h, \boldsymbol{\varphi}_{h^+} - \pi_h\boldsymbol{\varphi}))_K|}{Q(\boldsymbol{u}) - Q(\boldsymbol{u}_h)}, \tag{6.2}$$

i.e. the fraction between the error representation formula and the two primal problems is η_1 and the fraction between the error representation formula and the difference between the converged solution and the current FE solution is η_2. In order to present graphs of convergence rates, we also define the average size of the elements in the grid as

$$h_a = \frac{\mathrm{m}(\Omega)}{\sqrt{N_{el}}}, \tag{6.3}$$

where N_{el} is the number of elements in the current mesh and $\mathrm{m}(\Omega)$ is the area of the considered domain.

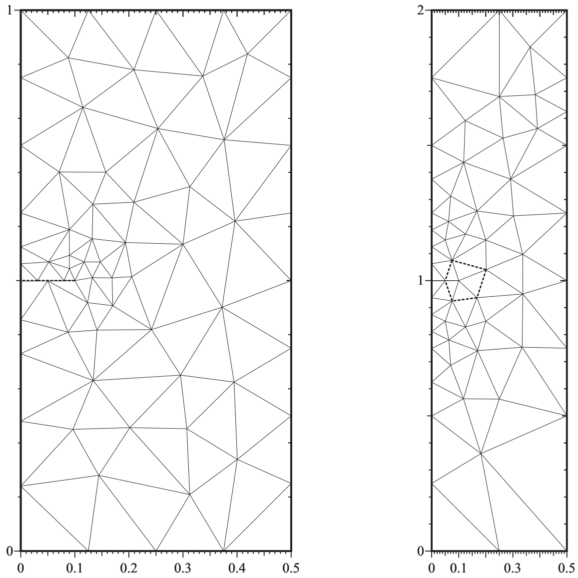

FIGURE 3. The initial grids. From left to right: 1) boundary movement and 2) contour and domain integrals.

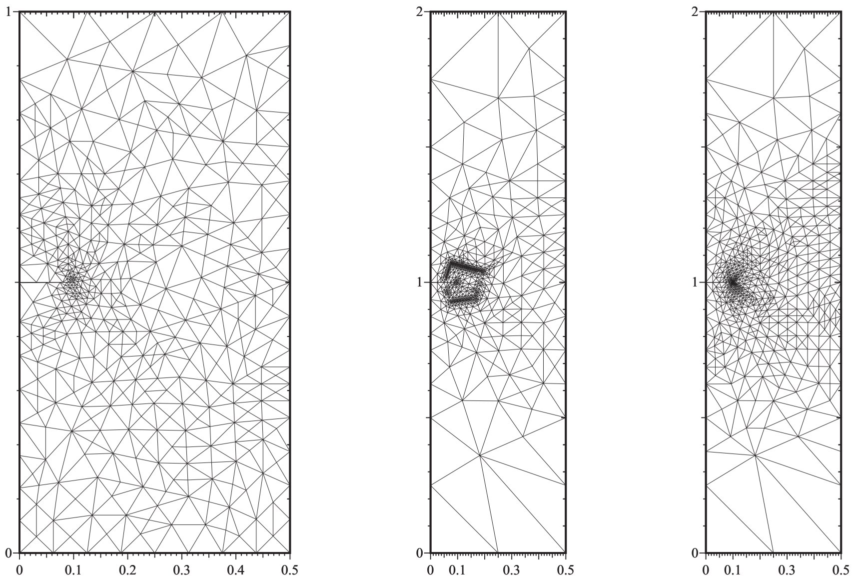

FIGURE 4. Example of adapted grids for the three goal-quantities satisfying $e_{rel} \leq 1\%$ for $p = 1$. From left to right: 1) boundary movement, 2) contour integral and 3) domain integral.

6.1. **Boundary movements.** The exact goal quantity, $Q(\boldsymbol{u})$, was approximated by a reference solution (an adaptive computation), which was considered accurate when eight decimal points did not change from one grid level to the next.

$$Q(\boldsymbol{u}) = 3.87362666\text{e-}07. \tag{6.4}$$

The convergence plots can be found in Fig. 5-6 and the computational results from each grid level are found in Table 1-3. Note that the convergence rate for $p = 2$ was highest for the primal problem of order $p + 1$ although the error representation formula is evaluated for the primal problem of order p. In the tables it is shown that $\eta_1 \approx 1$ in each iteration and $\eta_2 \to 1$ when $h \to 0$.

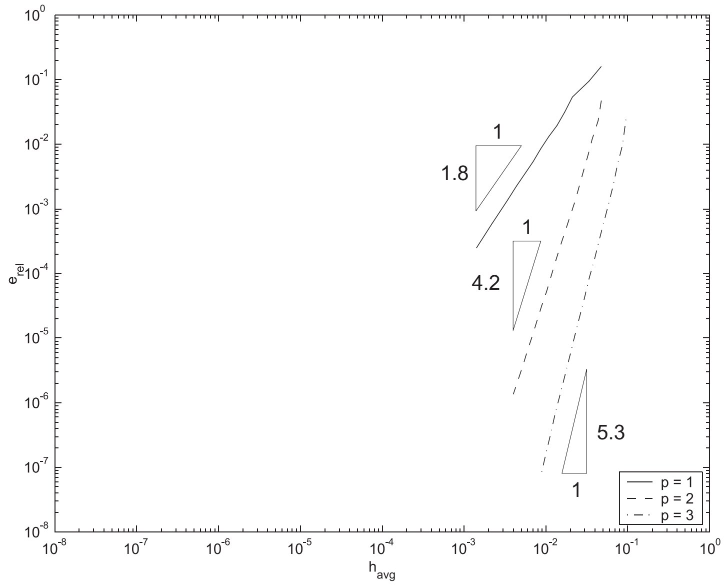

FIGURE 5. Convergence rates for boundary movement. The plot shows the convergence rate for the primal problem of order p.

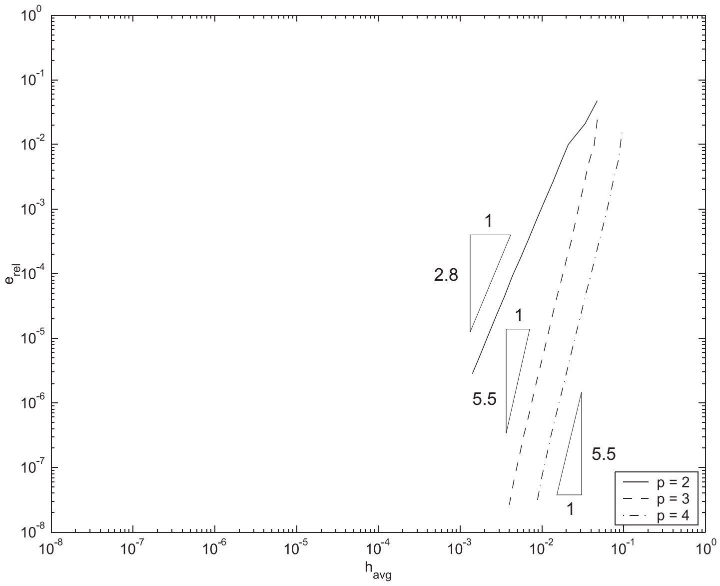

Figure 6. Convergence rates for boundary movement. The plot shows the convergence rate for the primal problem of order $p+1$.

Table 1. Computational results from crack boundary movement, grid order 1.

Elements	$Q(\boldsymbol{u}_h)$	$Q(\boldsymbol{u}_{h^+})$	$\lvert E(\boldsymbol{u},\boldsymbol{u}_h)\rvert$	$\boldsymbol{\eta}_1$	$\boldsymbol{\eta}_2$
110	3.2470737e-07	3.6897228e-07	4.4264914e-08	0.9999999999	0.7065
222	3.5041770e-07	3.7932268e-07	2.8904977e-08	1.0000000000	0.7824
557	3.6656617e-07	3.8347561e-07	1.6909443e-08	0.9999999999	0.8131
1342	3.7976045e-07	3.8633874e-07	6.5782904e-09	0.9999999999	0.8653
3339	3.8407979e-07	3.8709362e-07	3.0138285e-09	0.9999999997	0.9180
5155	3.8529673e-07	3.8722576e-07	1.9290278e-09	0.9999999997	0.9337
8198	3.8601221e-07	3.8729237e-07	1.2801606e-09	1.0000000000	0.9480
13052	3.8649024e-07	3.8732652e-07	8.3627845e-10	0.9999999995	0.9586
20467	3.8680692e-07	3.8734543e-07	5.3850860e-10	0.9999999998	0.9690
51340	3.8713365e-07	3.8735833e-07	2.2468676e-10	1.0000000044	0.9811
79581	3.8721281e-07	3.8736049e-07	1.4767762e-10	1.0000000126	0.9855
126163	3.8726668e-07	3.8736157e-07	9.4894016e-11	1.0000000142	0.9886

Table 2. Computational results from crack boundary movement, grid order 2.

Elements	$Q(\boldsymbol{u}_h)$	$Q(\boldsymbol{u}_{h^+})$	$\lvert E(\boldsymbol{u},\boldsymbol{u}_h)\rvert$	$\boldsymbol{\eta}_1$	$\boldsymbol{\eta}_2$
110	3.6897228e-07	3.7797897e-07	9.0066939e-09	1.0000000000	0.4898
186	3.8272093e-07	3.8549255e-07	2.7716175e-09	0.9999999999	0.5971
228	3.8466615e-07	3.8641076e-07	1.7446112e-09	1.0000000000	0.6470
375	3.8646710e-07	3.8711867e-07	6.5157643e-10	0.9999999997	0.7276
628	3.8706068e-07	3.8730052e-07	2.3984673e-10	0.9999999988	0.7942
1092	3.8725854e-07	3.8734687e-07	8.8328184e-11	1.0000000006	0.8484
1846	3.8732690e-07	3.8735866e-07	3.1757245e-11	0.9999999975	0.8881
3129	3.8735026e-07	3.8736165e-07	1.1390499e-11	0.9999999878	0.9188
5301	3.8735828e-07	3.8736241e-07	4.1318194e-12	0.9999997652	0.9437
9057	3.8736115e-07	3.8736260e-07	1.4505046e-12	1.0000000727	0.9619
11880	3.8736178e-07	3.8736263e-07	8.5942046e-13	0.9999992709	0.9706
15716	3.8736214e-07	3.8736265e-07	5.1071099e-13	0.9999984477	0.9804

Table 3. Computational results from crack boundary movement, grid order 3.

Elements	$Q(\boldsymbol{u}_h)$	$Q(\boldsymbol{u}_{h^+})$	$\lvert E(\boldsymbol{u},\boldsymbol{u}_h)\rvert$	$\boldsymbol{\eta}_1$	$\boldsymbol{\eta}_2$
110	3.7797897e-07	3.8149049e-07	3.5115211e-09	0.9999999999	0.3742
178	3.8548032e-07	3.8625209e-07	7.7177142e-10	0.9999999997	0.4100
284	3.8687293e-07	3.8708351e-07	2.1058209e-10	1.0000000015	0.4300
496	3.8723489e-07	3.8729265e-07	5.7758694e-11	1.0000000066	0.4521
874	3.8732943e-07	3.8734507e-07	1.5636286e-11	1.0000000509	0.4706
1487	3.8735421e-07	3.8735827e-07	4.0610846e-12	1.0000001066	0.4807
2547	3.8736049e-07	3.8736157e-07	1.0814523e-12	0.9999999896	0.4972
4382	3.8736212e-07	3.8736239e-07	2.7370127e-13	1.0000026648	0.5045
5756	3.8736238e-07	3.8736253e-07	1.4574396e-13	1.0000064598	0.5250
7549	3.8736253e-07	3.8736260e-07	6.9567750e-14	1.0000100432	0.5252
9886	3.8736260e-07	3.8736263e-07	3.5216445e-14	1.0000320363	0.5519
12967	3.8736263e-07	3.8736265e-07	1.8299579e-14	1.0000961506	0.6151

6.2. **Contour integral.** $E_S(\boldsymbol{u}, \boldsymbol{u}_h, \boldsymbol{v})$ was linearized using the midpoint rule (3.12) and two FEM solutions $\boldsymbol{u}_h$ and $\boldsymbol{u}_{h^+}$ obtained from the primal problem. This linearization is exact when $\boldsymbol{u}_{h^+} \to \boldsymbol{u}$ since the gradient of the goal quantity is linear in $\boldsymbol{u}$. The exact goal quantity was approximated by a reference solution (an adaptive computation), which was considered accurate if more than 245,000 degrees of freedom were used.

$$Q(\boldsymbol{u}) = 2.7933302. \tag{6.5}$$

The convergence plots can be found in Fig. 7-8 and the computational results from each grid level are found in Table 4-6. Note that the highest convergence rate was obtained with $p = 2$ for the primal problem of order $p + 1$. In the tables it is shown that $\eta_1 \approx 1$ in each iteration and $\eta_2 \to 1$ when $h \to 0$.

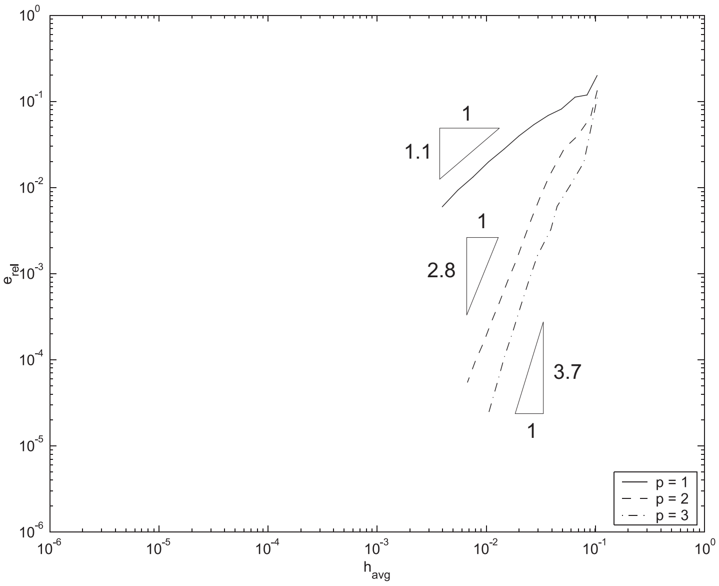

FIGURE 7. Convergence rates for the contour integral formulation of J. The plot shows the convergence rate for the primal problem of order p.

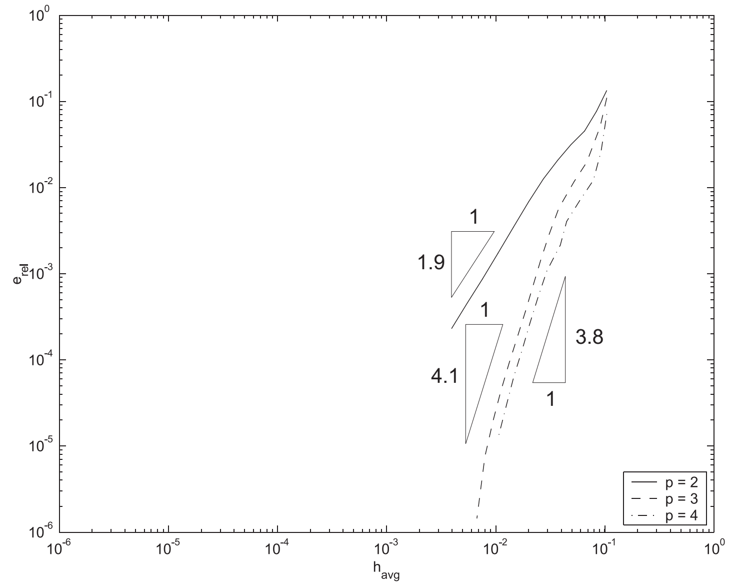

FIGURE 8. Convergence rates for the contour integral formulation of J. The plot shows the convergence rate for the primal problem of order $p+1$.

TABLE 4. Computational results from contour integral formulation for J, grid order 1.

Elements	$Q(\boldsymbol{u}_h)$	$Q(\boldsymbol{u}_{h^+})$	$\lvert E(\boldsymbol{u}, \boldsymbol{u}_h)\rvert$	$\boldsymbol{\eta}_1$	$\boldsymbol{\eta}_2$
92	2.2307057	2.4210364	0.1903306	1.0000000042	0.3726
141	2.4632842	2.5792784	0.1159941	1.0000000011	0.3757
235	2.4805871	2.6667239	0.1861367	0.9999999998	0.5951
422	2.5667342	2.7054665	0.1387322	0.9999999994	0.6122
728	2.6013540	2.7356237	0.1342697	1.0000000002	0.6994
1335	2.6426613	2.7581183	0.1154569	1.0000000015	0.7662
2508	2.6828502	2.7742395	0.0913892	0.9999999982	0.8272
4747	2.7159805	2.7836601	0.0676795	0.9999999990	0.8749
9110	2.7379917	2.7885265	0.0505347	0.9999999984	0.9131
17431	2.7564915	2.7909162	0.0344246	1.0000000093	0.9344
33292	2.7673576	2.7920464	0.0246887	0.9999999967	0.9505
64437	2.7768378	2.7926880	0.0158502	0.9999999954	0.9610

Table 5. Computational results from contour integral formulation for J, grid order 2.

Elements	$Q(\boldsymbol{u}_h)$	$Q(\boldsymbol{u}_{h^+})$	$\lvert E(\boldsymbol{u},\boldsymbol{u}_h)\rvert$	$\boldsymbol{\eta}_1$	$\boldsymbol{\eta}_2$
92	2.4210364	2.4853275	0.0642910	0.9999999993	0.1726
214	2.6834643	2.7385756	0.0551112	0.9999999990	0.5016
691	2.7552744	2.7772829	0.0220085	1.0000000050	0.5783
1478	2.7812707	2.7892570	0.0079863	1.0000000068	0.6622
2057	2.7864612	2.7912900	0.0048288	1.0000000041	0.7029
2830	2.7894359	2.7923135	0.0028775	0.9999999997	0.7389
4005	2.7910057	2.7928170	0.0018113	0.9999999664	0.7792
5699	2.7920445	2.7930799	0.0010354	1.0000000855	0.8053
8101	2.7925676	2.7932100	0.0006423	1.0000003725	0.8424
11223	2.7928889	2.7932757	0.0003867	1.0000004530	0.8765
15736	2.7930608	2.7933092	0.0002483	0.9999991754	0.9220
22072	2.7931782	2.7933262	0.0001479	0.9999992591	0.9736

Table 6. Computational results from contour integral formulation for J, grid order 3.

Elements	$Q(\boldsymbol{u}_h)$	$Q(\boldsymbol{u}_{h^+})$	$\lvert E(\boldsymbol{u},\boldsymbol{u}_h)\rvert$	$\boldsymbol{\eta}_1$	$\boldsymbol{\eta}_2$
92	2.4853275	2.5935380	0.1082105	1.0000000099	0.3513
163	2.7386567	2.7595958	0.0209391	1.0000000021	0.3829
289	2.7639836	2.7737680	0.0097844	1.0000000102	0.3334
504	2.7765150	2.7821144	0.0055993	1.0000000048	0.3329
650	2.7843022	2.7873241	0.0030218	0.9999999913	0.3347
1146	2.7888066	2.7903305	0.0015238	1.0000000198	0.3368
1666	2.7910520	2.7918340	0.0007820	1.0000000691	0.3432
2362	2.7921750	2.7925857	0.0004107	1.0000001502	0.3555
3246	2.7927383	2.7929618	0.0002235	0.9999998789	0.3776
4671	2.7930295	2.7931511	0.0001216	0.9999995979	0.4044
6320	2.7931839	2.7932470	0.0000630	0.9999995878	0.4311
8904	2.7932617	2.7932949	0.0000331	0.9999991291	0.4846

6.3. **Domain Integral.** $E_S(\boldsymbol{u}, \boldsymbol{u}_h, \boldsymbol{v})$ was linearized using the midpoint rule (3.12) and two FEM solutions $\boldsymbol{u}_h$ and $\boldsymbol{u}_{h^+}$ obtained from the primal problem. This linearization is exact when $\boldsymbol{u}_{h^+} \to \boldsymbol{u}$ since the gradient of the goal quantity is linear in $\boldsymbol{u}$. The exact goal quantity was approximated by a reference solution, which was considered accurate if more than $245,000$ degrees of freedom were used.

$$Q(\boldsymbol{u}) = 2.7953116. \tag{6.6}$$

The convergence plots can be found in Fig. 9-10 and the computational results from each grid level are found in Table 7-9. In the tables it is shown that $\eta_1 \approx 1$ in each iteration and $\eta_2 \to 1$ when $h \to 0$.

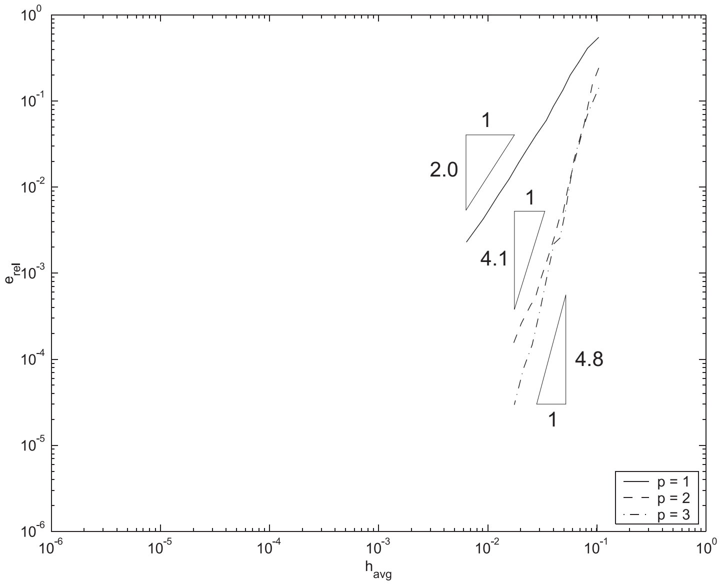

FIGURE 9. Convergence rates for the domain integral formulation for J. The plot shows the convergence rate for the primal problem of order p.

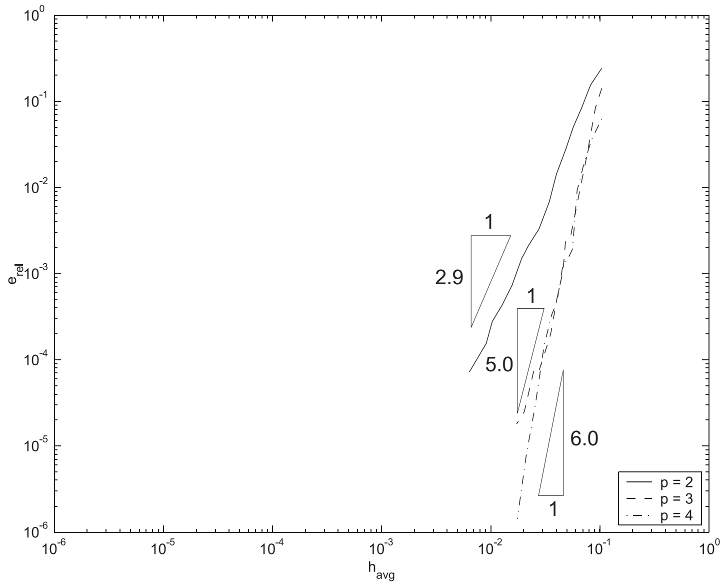

FIGURE 10. Convergence rates for the domain integral formulation for J. The plot shows the convergence rate for the primal problem of order $p+1$.

TABLE 7. Computational results from domain integral formulation for J, grid order 1.

Elements	$Q(\boldsymbol{u}_h)$	$Q(\boldsymbol{u}_{h^+})$	$\lvert E(\boldsymbol{u},\boldsymbol{u}_h)\rvert$	$\boldsymbol{\eta}_1$	$\boldsymbol{\eta}_2$
92	1.2603528	2.1181038	0.8577509	1.0000000859	0.5588
214	2.0081166	2.5585300	0.5504134	0.9999999639	0.6992
422	2.4204708	2.7171223	0.2966515	1.0000000900	0.7914
848	2.6288955	2.7761531	0.1472576	0.9999999534	0.8848
1288	2.6835723	2.7860932	0.1025209	1.0000000261	0.9175
2017	2.7235815	2.7893676	0.0657861	0.9999999818	0.9171
2707	2.7419812	2.7911595	0.0491783	1.0000000567	0.9221
4048	2.7607484	2.7932546	0.0325061	1.0000000186	0.9404
6269	2.7723227	2.7941232	0.0218004	0.9999999266	0.9483
9420	2.7799192	2.7945339	0.0146146	0.9999999265	0.9494
11955	2.7833939	2.7948796	0.0114856	1.0000000257	0.9637
24551	2.7888859	2.7951095	0.0062235	1.0000000571	0.9685

TABLE 8. Computational results from domain integral formulation for J, grid order 2.

Elements	$Q(\boldsymbol{u}_h)$	$Q(\boldsymbol{u}_{h^+})$	$\|E(\boldsymbol{u},\boldsymbol{u}_h)\|$	$\boldsymbol{\eta}_1$	$\boldsymbol{\eta}_2$
92	2.1181038	2.3984536	0.2803498	0.9999999825	0.4139
143	2.5399996	2.6687119	0.1287123	0.9999999358	0.5041
215	2.7105665	2.7620830	0.0515164	1.0000000643	0.6078
344	2.7698200	2.7879205	0.0181004	0.9999999745	0.7100
475	2.7824413	2.7923274	0.0098860	1.0000000643	0.7681
604	2.7882123	2.7938641	0.0056517	1.0000000363	0.7961
791	2.7911423	2.7947540	0.0036116	1.0000000312	0.8662
1066	2.7929266	2.7950048	0.0020781	1.0000000012	0.8713
1349	2.7939043	2.7951188	0.0012144	1.0000000732	0.8630
1626	2.7941123	2.7951039	0.0009915	1.0000000143	0.8268
2438	2.7945822	2.7952415	0.0006593	0.9999999454	0.9040
3345	2.7948822	2.7952615	0.0003793	0.9999999778	0.8835

TABLE 9. Computational results from domain integral formulation for J, grid order 3.

Elements	$Q(\boldsymbol{u}_h)$	$Q(\boldsymbol{u}_{h^+})$	$\|E(\boldsymbol{u},\boldsymbol{u}_h)\|$	$\boldsymbol{\eta}_1$	$\boldsymbol{\eta}_2$
92	2.3984536	2.6200230	0.2215694	0.9999999809	0.5583
198	2.6818958	2.7429445	0.0610486	1.0000000173	0.5382
259	2.7367694	2.7696508	0.0328814	0.9999999829	0.5616
315	2.7663056	2.7899287	0.0236230	1.0000000994	0.8144
372	2.7802803	2.7910154	0.0107351	1.0000000439	0.7141
474	2.7881684	2.7917051	0.0035367	1.0000000340	0.4951
609	2.7891561	2.7939933	0.0048371	0.9999999685	0.7858
773	2.7922262	2.7943989	0.0021726	0.9999999634	0.7041
1054	2.7941382	2.7949109	0.0007727	1.0000000393	0.6585
1520	2.7948973	2.7952293	0.0003320	1.0000000591	0.8015
2204	2.7950967	2.7952893	0.0001926	0.9999999880	0.8964
3234	2.7952288	2.7953075	0.0000787	1.0000000381	0.9517

7. Concluding remarks

In the plots we have seen that the convergence rates for elements with higher approximation order ($p = 3, 4$) are influenced by the regularity of the solution (singularity at the crack tip), and does not always realize the theoretical predictions. Higher convergence rates might be obtained with the development of anisotropic mesh refinement algorithms that are more adaptive.

We have also shown that the ratio between the error representation formula and the difference between the two primal problems (η_1) is close to one in each iteration. Therefore, we can say that the error estimate is in a sense trivial and that the error representation formula is more a tool to put high quality indicators on the elements for the refinement to the next grid level. This is the case for many engineering quantities such as stresses, strains and strain energy, which are at most quadratic in the solution. This can be used during the implementation to test the code. Solve two primal problems in $\boldsymbol{V}_h$ and $\boldsymbol{V}_{h^+}$ and solve the dual problem in $\boldsymbol{V}_{h^+}$, then

$$\frac{|\sum_{K\in T_h}(L(\boldsymbol{\varphi}_{h^+} - \pi_h\boldsymbol{\varphi}) - a(\boldsymbol{u}_h, \boldsymbol{\varphi}_{h^+} - \pi_h\boldsymbol{\varphi}))_K|}{Q(\boldsymbol{u}_{h^+}) - Q(\boldsymbol{u}_h)} \approx 1.0. \tag{7.1}$$

If this does not hold (and the code is free from bugs), underlying reasons can be

- Wrong linearization of $E_S(\boldsymbol{u}, \boldsymbol{u}_h; \boldsymbol{v})$.
- Wrong quadrature—raise the quadrature order.
- Decrease the tolerance on the residual in the iterative solver.
- Floating point representation in the computer.

The overhead cost of the evaluation of two primal problems is high, but on the other hand one can use the result of the finer primal problem. This solution is clearly more accurate, but on the other hand the error representation is less correct than for the coarse solution. In the numerical examples we have seen that the best overall results have been obtained with $p = 2$ for the primal and $p = 3$ for the dual problem.

In a complex time dependent simulation, involving propagating cracks, it is difficult, or indeed impossible, to design a mesh that is appropriate for the whole simulation. By using an adaptive scheme we might alleviate this difficulty since the mesh is adapted in an ' automatic' fashion during the simulation. Reliable numerical results can be obtained and an effective use of the degrees of freedom in the problem is ensured.

References

[1] K. Eriksson, D. Estep, P. Hansbo, and C. Johnson. *Computational Differential Equations.* Cambridge University Press, 1996.

[2] K. Eriksson, D. Estep, P. Hansbo, and C. Johnson. Introduction to adaptive methods for differential equations. *Acta Numerica*, pp105-158, 1995.

[3] C. Johnson and P. Hansbo. Adaptive finite element methods in computational mechanics *Comput. Methods Appl. Mech. Engrg*, (101):143-181, 1992.

[4] R. Becker and R. Rannacher. A feed-back approach to error control in finite element methods: basic analysis and examples. *East-West J. Numer. Math.*, (4):237-264, 1996.

[5] R. Rannacher and F.-T. Suttmeier. A feed-back approach to error control in finite element methods: application to linear elasticity. *Computational Mechanics*, (19):434–446, 1997.

[6] F. Larsson. *Goal-oriented error measures and adaptive finite element procedures in solid mechanics.* lic. thesis, Chalmers, 2001.

[7] J.R Rice. A path independent integral and the approximate analysis of strain concentration by notches and cracks. *Journal of Applied Mechanics*, 35:379–386, 1968.

[8] F.Z. Li, C.F. Shih, A. Needleman, *A comparison of methods for calculating energy release rates*, Engr. Fract. Mech, 21, (1985), 405-421

[9] C.F. Shih, B. Moran, T. Nakamura, *Energy release rate along a three-dimensional crack front in a thermally stressed body*, Int. J. Fract., 30, (1986), 79-102

[10] M. Larson and J. Niklasson. A posteriori error estimation of functionals in elliptic problems: Experiments. Technical report, Chalmers Finite Element Center, 2001. PREPRINT 2001-04.

[11] H. Tada, P.C. Paris and G.R. Irwin. *The stress analysis of cracks handbook, third edition* Asme press 2000.

Chalmers Finite Element Center Preprints

2001–01 *A simple nonconforming bilinear element for the elasticity problem*
Peter Hansbo and Mats G. Larson

2001–02 *The $\mathcal{LL}^*$ finite element method and multigrid for the magnetostatic problem*
Rickard Bergström, Mats G. Larson, and Klas Samuelsson

2001–03 *The Fokker-Planck operator as an asymptotic limit in anisotropic media*
Mohammad Asadzadeh

2001–04 *A posteriori error estimation of functionals in elliptic problems: experiments*
Mats G. Larson and A. Jonas Niklasson

2001–05 *A note on energy conservation for Hamiltonian systems using continuous time finite elements*
Peter Hansbo

2001–06 *Stationary level set method for modelling sharp interfaces in groundwater flow*
Nahidh Sharif and Nils-Erik Wiberg

2001–07 *Integration methods for the calculation of the magnetostatic field due to coils*
Marzia Fontana

2001–08 *Adaptive finite element computation of 3D magnetostatic problems in potential formulation*
Marzia Fontana

2001–09 *Multi-adaptive galerkin methods for ODEs I: theory & algorithms*
Anders Logg

2001–10 *Multi-adaptive galerkin methods for ODEs II: applications*
Anders Logg

2001–11 *Energy norm a posteriori error estimation for discontinuous Galerkin methods*
Roland Becker, Peter Hansbo, and Mats G. Larson

2001–12 *Analysis of a family of discontinuous Galerkin methods for elliptic problems: the one dimensional case*
Mats G. Larson and A. Jonas Niklasson

2001–13 *Analysis of a nonsymmetric discontinuous Galerkin method for elliptic problems: stability and energy error estimates*
Mats G. Larson and A. Jonas Niklasson

2001–14 *A hybrid method for the wave equation*
Larisa Beilina, Klas Samuelsson and Krister Åhlander

2001–15 *A finite element method for domain decomposition with non-matching grids*
Roland Becker, Peter Hansbo and Rolf Stenberg

2001–16 *Application of stable FEM-FDTD hybrid to scattering problems*
Thomas Rylander and Anders Bondeson

2001–17 *Eddy current computations using adaptive grids and edge elements*
Y. Q. Liu, A. Bondeson, R. Bergström, C. Johnson, M. G. Larson, and K. Samuelsson

2001–18 *Adaptive finite element methods for incompressible fluid flow*
Johan Hoffman and Claes Johnson

2001–19 *Dynamic subgrid modeling for time dependent convection–diffusion–reaction equations with fractal solutions*
Johan Hoffman

2001–20 *Topics in adaptive computational methods for differential equations*
Claes Johnson, Johan Hoffman and Anders Logg

2001–21 *An unfitted finite element method for elliptic interface problems*
Anita Hansbo and Peter Hansbo

2001–22 *A P^2–continuous, P^1–discontinuous finite element method for the Mindlin-Reissner plate model*
Peter Hansbo and Mats G. Larson

2002–01 *Approximation of time derivatives for parabolic equations in Banach space: constant time steps*
Yubin Yan

2002–02 *Approximation of time derivatives for parabolic equations in Banach space: variable time steps*
Yubin Yan

2002–03 *Stability of explicit-implicit hybrid time-stepping schemes for Maxwell's equations*
Thomas Rylander and Anders Bondeson

2002–04 *A computational study of transition to turbulence in shear flow*
Johan Hoffman and Claes Johnson

2002–05 *Adaptive hybrid FEM/FDM methods for inverse scattering problems*
Larisa Beilina

2002–06 *DOLFIN - Dynamic Object oriented Library for FINite element computation*
Johan Hoffman and Anders Logg

2002–07 *Explicit time-stepping for stiff ODEs*
Kenneth Eriksson, Claes Johnson and Anders Logg

2002–08 *Adaptive finite element methods for turbulent flow*
Johan Hoffman

2002–09 *Adaptive multiscale computational modeling of complex incompressible fluid flow*
Johan Hoffman and Claes Johnson

2002–10 *Least-squares finite element method with applications in electromagnetics*
Rickard Bergström

2002–11 *Discontinuous/continuous least-squares finite element methods for Elliptic Problems*
Rickard Bergström and Mats G. Larson

2002–12 *Discontinuous least-squares finiteeElement methods for the Div-Curl problem*
Rickard Bergström and Mats G. Larson

2002–13 *Object oriented implementation of a general finite element code*
Rickard Bergström

2002–14 *On adaptive strategies and error control in fracture mechanics*
Per Heintz and Klas Samuelsson

These preprints can be obtained from

`www.phi.chalmers.se/preprints`